

Automated Feature Tracking for Real-Time Kinematic Analysis and Shape Estimation of Carbon Nanotube Growth

Kaveh Safavigerdini¹
Filiz Bunyak¹

Ramakrishna Surya¹
Matthew R. Maschmann¹

Jaired Collins¹
Kannappan Palaniappan¹

Prasad Calyam¹

¹University of Missouri-Columbia, USA

{ksgh2, rst7b, jrcqw5, calyamp, bunyak, maschmannm, pal}@missouri.edu

Abstract

Carbon nanotubes (CNTs) are critical building blocks in nanotechnology, yet the characterization of their dynamic growth is limited by the experimental challenges in nanoscale motion measurement using scanning electron microscopy (SEM) imaging. Existing *ex situ* methods offer only static analysis, while *in situ* techniques often require manual initialization and lack continuous per-particle trajectory decomposition. We present Visual Feature Tracking (VFTrack) an *in-situ* real-time particle tracking framework that automatically detects and tracks individual CNT particles in SEM image sequences. VFTrack integrates hand-crafted or deep feature detectors and matchers within a particle tracking framework to enable kinematic analysis of CNT micropillar growth. A systematic using 13,540 manually annotated trajectories identifies the ALIKED detector with LightGlue matcher as an optimal combination (F1-score of 0.78, α -score of 0.89). VFTrack motion vectors decomposed into axial growth, lateral drift, and oscillations, facilitate the calculation of heterogeneous regional growth rates and the reconstruction of evolving CNT pillar morphologies. This work enables advancement in automated nano-material characterization, bridging the gap between physics-based models and experimental observation to enable real-time optimization of CNT synthesis. Our source code is available at <https://github.com/kavehsfv/VFTrack>.

1. Introduction

Carbon Nanotubes (CNTs) are pivotal in advancing nanotechnology across electronics, materials science [28], optics [29], and polymer composites [6, 30] due to their superior electrical conductivity [19, 36, 51], mechanical robustness, and unique chemical properties [5, 9, 11]. These graphene-based tubular structures are synthesized as dense **CNT forest micropillars** [33, 35]—vertically aligned mi-

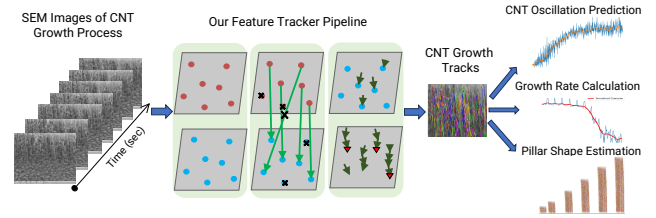


Figure 1. Overview of our VFTrack (particle) feature tracking pipeline that processes a sequence of SEM-based CNT growth images. Nanoscale CNT particles are automatically detected and tracked to quantify their oscillations and growth rates in real-time while reconstructing the evolving shape of the CNT micropillar.

croarchitectures exhibiting exceptional thermal/electrical conductivity, durability, and near-perfect optical absorption [32, 37, 42]. Understanding CNT micropillar growth dynamics requires advanced monitoring techniques [18, 22], categorized as **ex situ** methods analyzing static post-synthesis samples and **in situ** techniques monitoring real-time growth.

Ex situ mechanical characterization and static growth control techniques **fail to capture real-time CNT growth dynamics**. Shen et al. [41] employed nanoindentation and micropillar compression to link vertically aligned CNT orientation with anisotropic Young’s modulus, hardness, and fracture modes, but as an *ex-situ* technique, it cannot capture individual growth kinetics. Likewise, Zhou et al. [50] demonstrated static 3D architectures via orthogonal CVD growth, yet this approach offers no real-time view of morphological evolution or nanoscale fluctuations during synthesis.

In situ imaging approaches provide dynamic information but lack **continuous per-particle trajectory decomposition and oscillation analysis**. Adachi et al. [1] used *in situ* TEM to observe electromigration-driven sliding of Co nanorods inside MWCNTs and extract force parameters but did not extend to continuous tracking of growing CNT ensembles. Surya et al. [43, 44] applied ESEM

with digital image correlation and the Meta CoTracker algorithm to measure average forest growth rates under a rigid-body assumption, lacking per-particle trajectory decomposition or oscillation metrics. Pimonov et al. [34] demonstrated homodyne polarization microscopy for sub-second imaging of individual CNTs, revealing stochastic growth–pause–shrinkage switches but without mapping spatial drift or oscillation amplitudes in SEM frames. On the modeling side, Eltaher et al. [14] developed a doublet-based Timoshenko beam theory to predict CNT dynamic response under moving loads, yet this framework remains purely theoretical and disconnected from experimental image sequences.

Existing approaches to analyzing CNT kinematic properties are largely **manual and offline**, lacking automation and real-time responsiveness. Most current methods require manual seed selection and post-processing, preventing timely adjustments. In contrast, *real-time CNT investigation* enables live monitoring and adaptive control of experimental conditions such as temperature and pressure, facilitating the attainment of desired mechanical properties during growth.

Conventional computer vision solutions such as **particle tracking** [25, 31, 40], **cell tracking** [3, 7, 45] and **point tracking** [13, 20, 21] face inherent limitations in CNT video analysis. Particle tracking algorithms typically need manual initialization of particle locations and exhibit performance degradation over long image sequences, while point tracking methods require initial point selections and recurrent reinitialization for new features across frames, hindering scalability and robustness.

To address these gaps, we propose a robust, real-time image-based tracking framework. Our approach is built on a systematic evaluation of state-of-the-art feature detector [2, 8] (*SIFT* [26], *ALIKE* [49], *DISK* [46], *SuperPoint* [12]) and feature matcher [27, 39] (*SuperGlue* [38], *LightGlue* [24]). The framework is designed to automatically detect and match rich CNT particles across successive SEM frames, decompose their motions into growth, drift, and oscillation components, and reconstruct two-dimensional pillar morphologies.

The innovation of this study lies in three key areas that overcome the aforementioned limitations. First, our framework provides **fully automated tracking without manual initialization**, unlike conventional point-tracking methods that require seed selection. Second, it enables **continuous per-particle trajectory decomposition**, moving beyond simple growth rate averages to simultaneously quantify axial growth, lateral drift, and orientation oscillations. Third, its computational efficiency facilitates **real-time analysis and control**, creating the potential for adaptive optimization of synthesis conditions. Using this pipeline, researchers can implement closed-loop control

systems and apply different adaptive control theory models [47, 48] directly to their SEM machines for adaptive synthesis optimization. By integrating these capabilities, our methodology bridges the critical gap between theoretical dynamic models and experimental observation, as illustrated in Fig. 1, representing a significant advancement in automated nanomaterial characterization.

2. Methodology

This section is organized into four primary parts. Initially, we describe SEM video acquisition of CNT growth under varied conditions; second, we introduce a novel feature-tracking algorithm for extracting CNT keypoint trajectories; third, we present a vector composition-based kinematic analysis to compute CNT displacements, orientations, growth rates, and oscillations; and fourth, we outline a pillar-shape estimation method that reconstructs CNT micropillar morphology by aggregating tracked movements over time.

2.1. Preparing SEM Videos of CNT Images

Carbon nanotubes were produced under a variety of growth conditions, encompassing alterations in temperature, substrate type, and growth methodologies, employing both fixed and floating catalyst chemical vapor deposition techniques. These methods enabled the creation of solid materials through gas-phase reactions, resulting in CNTs with unique mechanical properties influenced by the substrate and growth technique. The physical attributes of the carbon nanotubes were examined through desktop SEM imaging and nanoindentation tests. The SEM captures CNT images of the target area shown in Fig. 2 (a) at one frame every 2 seconds, used to analyze CNT kinematics in this study. Figure 2 (b) illustrates a sequence of SEM images showing significant changes in the kinematics of carbon nanotubes over time.

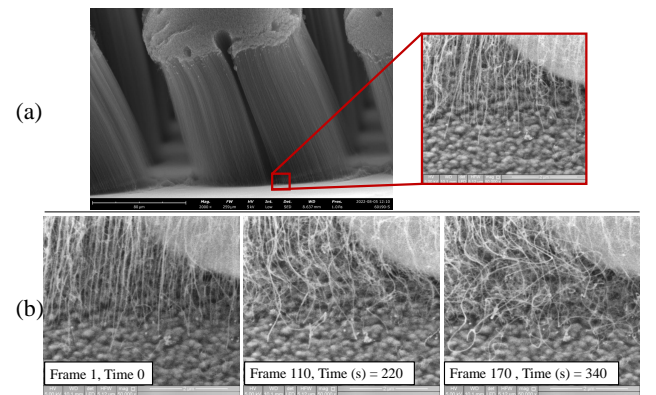


Figure 2. (a) Target area for frame capturing in the SEM imaging process, and (b) sample SEM image sequence showing notable changes in CNT kinematics.

2.2. Feature Tracking Algorithm

The feature tracking [15, 16] method aims to track and analyze keypoints movement across image sequences by identifying distinctive features in each frame, matching them, and recording their trajectories. The proposed algorithm integrates both traditional and contemporary techniques for feature detection and matching [17]. In this investigation, four distinct feature detection methods—SIFT, DISK, ALIKED, and SuperPoint—are coupled with the same matching method, LightGlue. The algorithm operates in five primary stages, as depicted in Fig. 3 and elaborated in Algorithm 1:

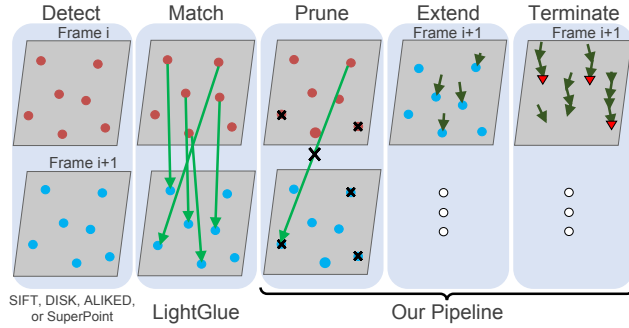


Figure 3. **Overview of VFTrack Framework:** **Detect:** Detection of features in subsequent frames using SIFT, DISK, ALIKED, or SuperPoint techniques. **Match:** Utilization of LightGlue for feature matching. **Prune:** Removal of keypoint mismatches and unpaired features. **Extend:** Formation of feature tracks and continue to grow as matched features are appended. **Terminate:** The algorithm considers tracks terminated (shown as red triangles) if no features match their heads and starts new tracks with the unmatched keypoints.

Detect: frame features were detected using the SIFT, DISK, ALIKED, or SuperPoint techniques (Algorithm 1, line 11).

Match: Feature matching is performed between consecutive frames using LightGlue, chosen for its speed and precision (Algorithm 1, line 12).

Prune: In this stage, the algorithm eliminates mismatches and unmatched features by enforcing a maximum displacement threshold between matched keypoints in consecutive frames. (Algorithm 2).

Extend [4, 23]: Tracks form and grow by appending matched features to existing tracks if they match the features at the head of the tracks (Algorithm 3).

Terminate: Finally, the algorithm terminates tracks if no features match their heads and starts new tracks with the unmatched keypoints. (Algorithm 4).

2.3. Kinematic Decomposition of Motion Vectors

The output of our visual feature tracking algorithm is a set of displacement vectors, one for each tracked CNT feature between consecutive frames. To extract meaningful phys-

Algorithm 1 Feature Tracking Method

Require: frames $frms$, feature $detector$, feature $matcher$
Ensure: Tracks $tracks$, keypoints kinematic $kptsKmts$, track id $trkID$, and keypoints track id map $kpTrkId$

```

1: Initialize  $tracks$ ,  $prvKpts$ ,  $kptsKmts$ ,  $kpTrkId \leftarrow \emptyset$ 
2:  $kpts0 \leftarrow detector(frms[0])$ ,  $dist\_th \leftarrow 40$ ,  $trkID \leftarrow 0$ 
3: for each  $kp \in kpts0$  do
4:    $tracks[trkID] \leftarrow [kp]$ ,  $kpTrkId[kp] \leftarrow trkID$ 
5:    $trkID \leftarrow +1$ ,  $prvKpts \leftarrow kpts0$ 
6: end for
7: for each  $(i, frm) \in frms[1 : ]$  do
8:    $kpts \leftarrow Detect(frm)$ 
9:    $mtchKpts \leftarrow Match(kpts, prvKpts)$ 
10:   $mtchKpts \leftarrow Prune(mtchKpts, dist\_th)$ 
11:   $tracks, kptsKmts, kpTrkId \leftarrow$ 
    Extend( $mtchKpts$ ,  $kpTrkId$ ,  $tracks$ ,  $kptsKmts$ )
12:   $kpTrkId, trkID \leftarrow$ 
    Terminate( $mtchKpts$ ,  $kpTrkId$ ,  $trkID$ )
13:   $prvKpts \leftarrow kpts$ 
14: end for
```

Algorithm 2 Prune Function

Require: $mtchKpts$, $dist_th$

```

1: Function Prune( $mtchKpts$ ,  $dist\_th$ )
2: for each  $(kp1, kp2) \in mtchKpts$  do
3:   if Euclidean_Distance( $kp1, kp2$ ) >  $dist\_th$  then
4:     remove ( $kp1, kp2$ ) from  $mtchKpts$ 
5:   end if
6: end for
7: return  $mtchKpts$ 
```

Algorithm 3 Extend Function

Require: $mtchKpts$, $kpTrkId$, $tracks$, $kptsKmts$

```

1: Function Extend( $mtchKpts$ ,  $kpTrkId$ ,  $tracks$ ,  $kptsKmts$ )
2: for each  $(kp1, kp2) \in mtchKpts$  do
3:    $trkID \leftarrow kpTrkId[kp1]$ 
4:   append ( $kp1, kp2$ ) to  $tracks[trkID]$ 
5:    $kptsKmts[trkID] \leftarrow$ 
     calc_kinematic( $(kp1, kp2)$ ,  $tracks[trkID]$ )
6:    $kpTrkId[kp2] \leftarrow trkID$ 
7: end for
8: return  $tracks, kptsKmts, kpTrkId$ 
```

ical insights, we decompose each raw displacement vector into components that represent distinct kinematic phenomena: axial growth, lateral drift, and oscillation.

As illustrated in Figure 4, each displacement vector is resolved into a vertical component (ΔY) and a horizontal component (ΔX) relative to the SEM image frame. We interpret the vertical displacement, ΔY , as the pri-

Algorithm 4 Terminate Function

Require: $mtchKpts, kpTrkId, trkID$

- 1: **Function Terminate**($mtchKpts, kpTrkId, trkID$)
 - 2: **for each** ($kp1, kp2$) **not in** $mtchKpts$ **do**
 - 3: $kpTrkId \leftarrow kpTrkId \setminus \{kp1\}, trkID \leftarrow +1$
 - 4: **append** ($trkID, kp2$) **to** $kpTrkId$
 - 5: **end for**
 - 6: **return** $kpTrkId, trkID$
-

mary **growth** component along the pillar's main axis. The horizontal displacement, ΔX , captures lateral movements, which we attribute to a combination of systemic **drift** of the entire pillar and localized **oscillations** of individual CNTs.

From these Cartesian components, we calculate the total displacement magnitude (l) and the instantaneous angle of motion (θ) relative to the vertical growth axis using the following standard transformations:

$$l = \sqrt{(\Delta X)^2 + (\Delta Y)^2} \quad (1)$$

$$\theta = \text{atan2}(\Delta X, \Delta Y) \quad (2)$$

Here, l represents the total distance a feature moved in a single time step, while θ quantifies its deviation from a purely vertical growth path. The temporal analysis of ΔY across all tracks yields the average growth rate, while the distribution and evolution of θ for individual tracks are used to characterize CNT oscillations.

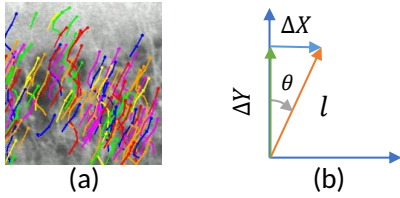


Figure 4. Decomposition of a CNT feature's motion vector. (a) Raw displacement vectors tracked between frames. (b) Each velocity vector is resolved into a vertical component (ΔY), representing growth, and a horizontal component (ΔX), representing drift and oscillation. The magnitude (l) and angle (θ) are calculated from these components.

2.4. Pillar Shape Estimation Methodology

Estimating the three-dimensional morphology of carbon nanotube (CNT) micropillars is crucial for linking their structure to their mechanical and electrical properties. We propose a method to reconstruct the pillar shape by sequentially stacking the 2D CNT track data obtained from in-situ SEM video frames. The method operates on the key assumption that once nanotubes grow beyond the initial nucleation zone (Fig. 2), their collective structure behaves as a

rigid body. In our iterative process, the algorithm first computes the average displacement vector (encompassing both growth and drift) from the tracked features in the current frame. This vector is then used to translate the entire previously reconstructed pillar shape. Finally, the new tracks from the current frame are superimposed at the pillar's base, representing the most recent growth. This layer-by-layer reconstruction is illustrated in Figure 5, which shows a final pillar built from a 100-frame sequence. The figure highlights how tracks from earlier frames (e.g., Frame 1) form the top of the pillar, while tracks from the final frame (Frame 100) constitute the growing base.

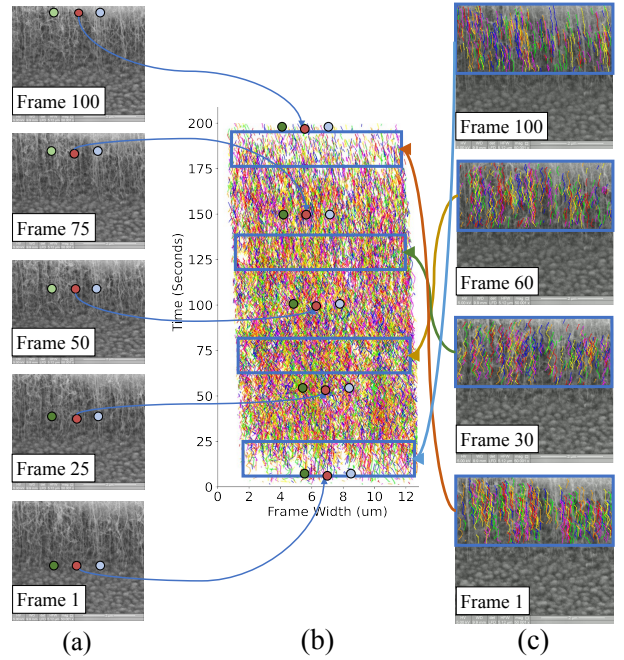


Figure 5. (a) CNT particles movement within the CNT micropillar over time. (b),(c): Visualizing the layer-by-layer reconstruction of a CNT micropillar. The method treats the collection of past tracks as a rigid body, which is shifted upward by the average growth and drift calculated for the current frame. The new tracks are then added to the base. This schematic shows the final positions of tracks from four sample frames (1, 30, 60, and 100) within a pillar constructed from a 100-frame sequence, mapping the temporal evolution into a final spatial structure.

3. Experiment Results

This section validates the proposed feature tracking framework through kinematic analysis of CNT growth. We evaluate different feature detector-matcher pipelines to identify the optimal configuration for accuracy and real-time performance, then apply this pipeline to extract key physical parameters including spatially-resolved growth rates and orientation fluctuations. Finally, we demonstrate the frame-

work’s ability to reconstruct evolving 2D pillar shapes, providing comprehensive insight into growth dynamics.

3.1. VFTrack Algorithm Performance Evaluation

We employed four feature extraction methods—SIFT, DISK, ALIKED, and SuperPoint—coupled with LightGlue as the matcher. For this evaluation, a comprehensive ground-truth dataset was created by manually annotating 13,540 individual CNT trajectories across five distinct growth videos; this annotation was cross-referenced with results from the Meta CoTracker [21] to ensure high fidelity. The performance of each pipeline was rigorously evaluated using the standardized software from the Particle Tracking Challenge [10]. While this framework provides several metrics (e.g., number of paired, generated, and missed tracks), we adopted the primary Jaccard similarity index, or α score, as the main indicator of tracking quality. The α -score quantifies the similarity between the set of ground-truth tracks (X) and the estimated tracks (Y) using the relation:

$$\alpha(X, Y) = 1 - \frac{d(X, Y)}{d(X, \emptyset)} \quad (3)$$

where $d(X, Y)$ is the cumulative error distance between matched tracks, and the denominator $d(X, \emptyset)$ serves as a normalization factor based on the total length of the ground-truth tracks [10]. The score ranges up to a maximum of 1, with a higher value indicating a closer approximation to the ground truth.

In addition, the following standard performance metrics were derived: precision, recall, and F1 score. These were computed using the formulas below:

$$\text{Precision} = \frac{\text{Paired Tracks (Alg., Ground Truth)}}{\text{Total Alg. Generated Tracks}}. \quad (4)$$

$$\text{Recall} = \frac{\text{Paired Tracks (Alg., Ground Truth)}}{\text{Total Ground Truth Tracks}}. \quad (5)$$

$$\text{F1 Score} = \frac{2 \times \text{Precision} \times \text{Recall}}{\text{Precision} + \text{Recall}}. \quad (6)$$

The performance of each feature extraction method combined with either SuperGlue or LightGlue was evaluated using these metrics, alongside the runtime (seconds) per frame, as summarized in Tab. 1. The results clearly indicate that the LightGlue matcher provides superior accuracy and speed compared to SuperGlue across all detectors. Among the tested combinations, the **ALIKED + LightGlue** pipeline (highlighted in the table) emerged as the optimal choice, achieving the highest scores across all accuracy metrics, including an F1-score of 0.78 and an α -score

of 0.89. Although the SuperPoint + LightGlue pairing was faster, its accuracy was significantly lower. The ALIKED + LightGlue combination thus represents the best trade-off, delivering state-of-the-art tracking fidelity with a runtime (0.31s) well-suited for real-time applications. Consequently, this pipeline was adopted for all subsequent analyses in this study.

Method	Prec.↑	Recall↑	F1↑	α ↑	Runtime↓
SuperPoint + SuperGlue	0.57	0.59	0.55	0.54	0.54
SIFT + SuperGlue	0.53	0.49	0.51	0.50	1.42
DISK + SuperGlue	0.59	0.55	0.57	0.61	3.77
ALIKED + SuperGlue	0.73	0.67	0.70	0.81	1.01
SuperPoint + LightGlue	0.64	0.66	0.62	0.63	0.18
SIFT + LightGlue	0.60	0.56	0.58	0.58	0.55
DISK + LightGlue	0.65	0.61	0.61	0.67	1.11
ALIKED + LightGlue	0.81	0.75	0.78	0.89	0.31

Table 1. Quantitative comparison of feature tracking pipelines, pairing four feature detectors with either the SuperGlue or LightGlue matcher. Performance is evaluated using precision, recall, F1-score, the α -score (higher is better), and average runtime per frame in seconds (lower is better). The combination of ALIKED and LightGlue (highlighted) achieves the highest tracking accuracy, establishing it as the optimal method.

Additionally, the average length and standard deviation (STD) of the generated tracks were considered as metrics for comparing the variations of these methods. A higher track length with a lower STD indicates that the method can track CNT movement for an extended period. The results, shown in Fig. 7, highlight that the SuperPoint and LightGlue combination performs well with a low number of keypoints per frame and maintains that performance even as the number of detected keypoints increases. Conversely, the DISK and LightGlue combination is the best option when dealing with a high number of keypoints per frame. The ALIKED+LightGlue combination offers the best balance and robustness in both low and high-density keypoint scenarios, making it versatile for a wide range of CNT dynamics in SEM imaging. Our analysis shows it consistently delivers reliable performance, balancing runtime efficiency with high tracking quality, making it the most effective approach across all feature densities.

Real-time capability: The proposed feature tracking algorithm demonstrates real-time compatibility for analyzing CNT kinematics in SEM microscopy, where SEM typically generates a frame every 2 seconds or less. As indicated in Tab. 1, our methods process each frame in under 1.1 seconds, even in the worst-case scenario (DISK + LightGlue). This means the algorithm is able to process a frame faster than the image acquisition rate of the SEM, ensuring seamless real-time operation. Furthermore, the SuperPoint + LightGlue method, with a processing time of 0.18 sec-

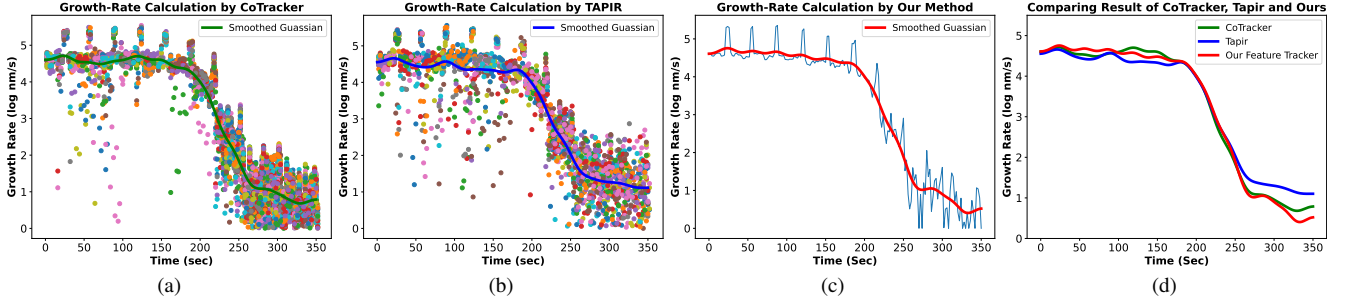


Figure 6. (a) CNT growth rate calculation using CoTracker. (b) CNT growth rate calculation using TAPIR. (c) CNT growth rate calculation using VFTrack algorithm. (d) Comparison of growth rate calculations by different methods.

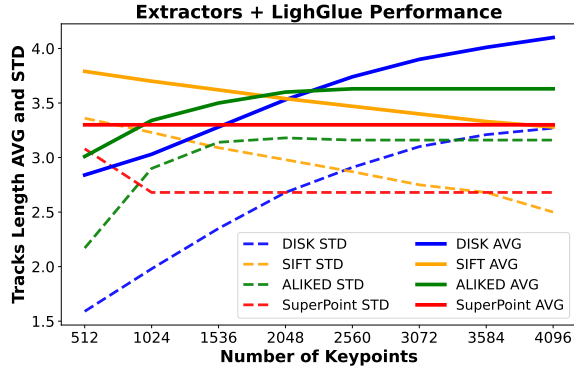


Figure 7. Comparison of average track length and standard deviation for feature tracking methods in SEM images. ALIKED + LightGlue shows the best overall performance, with SuperPoint + LightGlue excelling in low-density and DISK + LightGlue excelling in high-density keypoint scenarios.

onds per frame, stands out for ultra-fast real-time tracking applications.

3.2. CNT Growth Rate Calculation

The carbon nanotube growth rate, a vital parameter derived from our vector composition analysis in Sec. 2.3, was quantitatively evaluated using three distinct methods: two established point-tracking approaches (CoTracker [21] and TAPIR [13]) and our novel visual feature-tracking algorithm. For CoTracker and TAPIR, growth rates were calculated from 206 manually selected keypoints across SEM frames (Fig. 6a-b), while our automated approach (Fig. 6c) autonomously identifies tracking points. Figure 6d demonstrates our method’s superior growth rate estimation accuracy. Crucially, by eliminating manual keypoint initialization, our technique enables real-time CNT growth monitoring in SEM—a significant advancement over conventional point-tracking.

Regional Growth Rate Calculation: One of key advantage of the VFTrack method is its capacity to calculate growth rates within *arbitrary regions* of SEM image se-

quences, as demonstrated in Fig. 8. This capability captures complex CNT dynamics and evolving growth patterns across different sections of CNT micropillars over time.

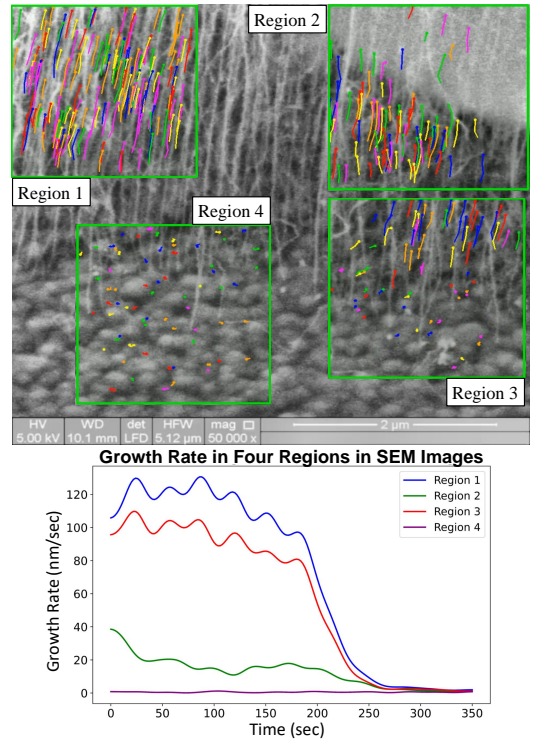


Figure 8. Spatially resolved growth rate analysis using our visual feature-tracking method. By defining four distinct regions, the algorithm reveals significant heterogeneity in the growth dynamics across the CNT pillar, a key advantage over global or sparse-point tracking methods.

3.3. Temporal Analysis of CNT Tracks’ Orientation

Building on the vector composition analysis in Sec. 2.3, the temporal evolution of Carbon Nanotube (CNT) orientation offers deeper insight into their dynamic behavior. By leveraging feature tracking, the orientation θ of CNT tracks are

continuously monitored relative to a vertical reference. As shown in Fig. 9 the mean orientation of the tracked CNTs is observed to fluctuate around zero degrees, indicating that, on average, the CNTs tend to align vertically.

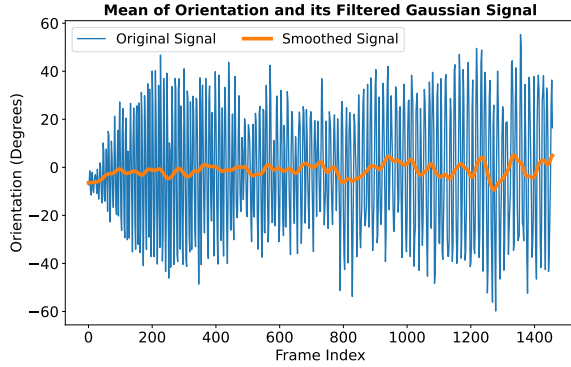


Figure 9. Mean orientation of carbon nanotubes over time, showing a general tendency to align vertically.

However, the standard deviation of these orientations shows an increasing trend in fluctuation magnitude, as seen in Fig. 10. It rises from nearly zero, indicating minimal initial deviation, to about 50 degrees in the later frames.

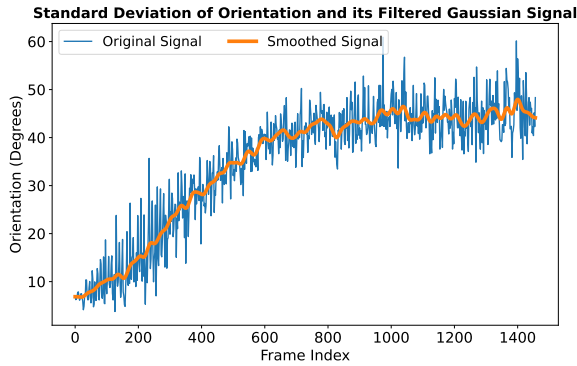


Figure 10. Increasing trend in the standard deviation of CNT orientations, rising from nearly zero to 50 degrees.

The high fluctuation of CNTs and the decrease in their growth rate towards the end of the experiment can be attributed to several factors. Growing CNTs requires specific conditions, particularly the controlled flow of carbon-containing gas over a substrate at precise pressure and temperature. Initially, these conditions facilitate a high growth rate, forming a dense micropillar of CNTs. However, as the CNTs continue to grow and the pillar becomes taller, the increasing weight at the top creates a mechanical load and reduces the available space on the substrate for new CNTs to form. Additionally, variations in temperature, pressure, and carbonated gas flow at the substrate level become more pronounced, leading to the formation of fewer, thinner, and sparser CNTs at the base. This reduced density at the base,

combined with the increased weight at the top, promotes the interconnection of CNTs, causing individual CNTs to deviate from their initial growth paths. These deviations result in significant fluctuations and oscillations in their structure, ultimately decreasing the overall growth rate and compromising the stability of the CNT structure.

3.4. Pillar Shape Estimation Results

Methodology of pillar shape estimation was introduced in Sec. 2.4. Figure 11, demonstrates the incremental expansion of a single micropillar base within a CNT image sequence over 1000 seconds which reveals a steady increase in vertical growth. Same procedure was applied to five distinct image sequences, with the results illustrated in Fig. 12. The figure illustrates both the growth height and the horizontal drift of the CNT micropillar, measured in micrometers. The results indicate that even minor changes in horizontal drift can significantly alter the final shape of the micropillar, potentially leading to substantial changes in the mechanical properties of the CNTs. The procedure was applied to five distinct image sequences, with the results illustrated in Fig. 12. The figure illustrates both the growth height and the horizontal drift of the CNT micropillar, measured in micrometers.

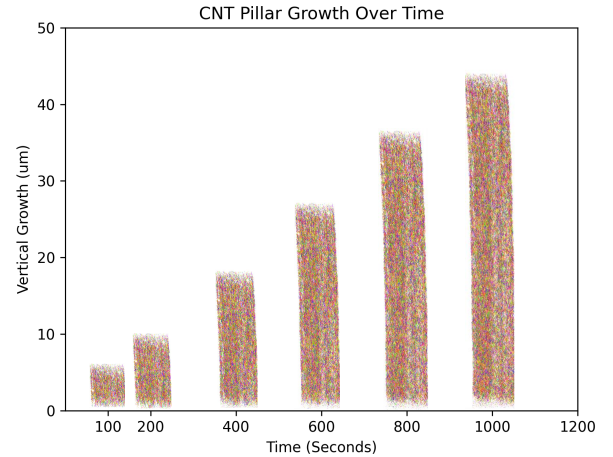


Figure 11. Time-lapse visualization of a CNT micropillar's expansion over 1000 seconds, showing steady increases in vertical growth.

Both steady vertical growth and noticeable horizontal drift are observed in the real CNT micropillar as depicted in Fig. 13. Images (a) through (c) illustrate the increasing height of the micropillar over time, while image (d) clearly shows the noticeable horizontal drift over time. The results demonstrate the effectiveness of the proposed method in estimating the shape of the CNT micropillar, providing valuable insights into the growth dynamics of CNTs in experimental settings.

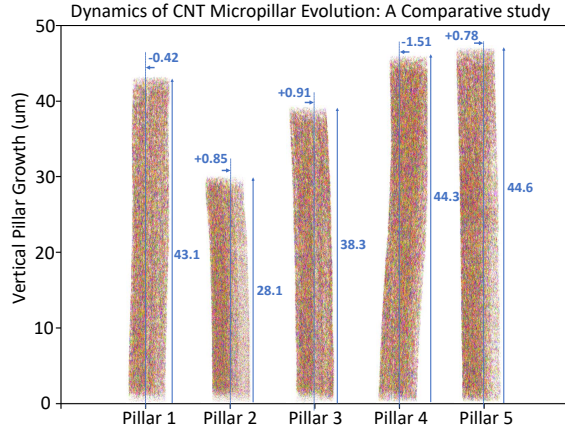


Figure 12. Comparative analysis of growth height and horizontal drift in CNT micropillars across five distinct image sequences.

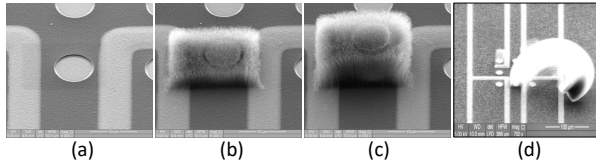


Figure 13. (a-c): Sequential images showing CNT micropillar's vertical growth. (d): Noticeable horizontal drift over time.

4. Conclusion and Future Works

In this work, we presented a novel, real-time feature-tracking framework designed to overcome the limitations of traditional ex situ and manual in situ methods for analyzing Carbon Nanotube (CNT) micropillar growth. Our comprehensive evaluation established the ALIKED detector paired with the LightGlue matcher as the optimal pipeline. By automatically detecting and tracking dense CNT particles, our method enables unprecedented kinematic analysis, including the decomposition of motion into growth, drift, and oscillation components, and the ability to compute regional growth rates. The successful reconstruction of evolving pillar morphologies, which captured both vertical growth and horizontal drift, further validates the framework's utility.

The findings have significant implications for nanotechnology applications, particularly in fields requiring precise control of CNT behavior. Real-time monitoring of CNT growth can lead to more reliable flexible electronic components, optimized aerospace materials, and enhanced medical devices. Additionally, understanding CNT dynamics can improve the fabrication of CNT-based transistors, structural health monitoring systems, and environmental sensors.

However, integrating these insights into existing technologies presents challenges, including the need for significant computational resources and the high cost and time of real-time SEM experiments. Environmental factors like

temperature and humidity also influence CNT behavior, requiring adaptive algorithms for accurate monitoring. Despite these challenges, our innovative methodology allows for a previously challenging level of detail precision in tracking CNT growth and behavior, providing dynamic insights into their mechanical properties. This knowledge can improve CNT-based products and lays a foundation for future research on environmental effects on CNT behavior, further advancing nanotechnology.

For future work, we plan to implement the algorithm on a local SEM machine for real-time data analysis, explore other feature extraction methods to enhance algorithm efficiency, and investigate the impact of environmental factors on CNT growth and movement. Combining advanced imaging with computational techniques, we anticipate further advancements in nanotechnology research and development of innovative CNT-based materials and devices.

Acknowledgments

All authors acknowledge the National Science Foundation grant CMMI-2026847 for funding. Any opinions, findings, and conclusions or recommendations expressed in this publication are those of the author(s) and do not necessarily reflect the views of the National Science Foundation.

References

- [1] Kensuke Adachi, Shogo Matsuyama, Yuki Sakai, and Hideo Kohno. Kinematics of electromigration-driven sliding of co nanorod fillers inside multi-walled carbon nanotubes. *Nanoscale Advances*, 2024. 1
- [2] Rumana Aktar, Hadi Aliakbarpour, Filiz Bunyak, Guna Seetharaman, and Kannappan Palaniappan. Performance evaluation of feature descriptors for aerial imagery mosaicking. In *IEEE Applied Imagery Pattern Recognition Workshop (AIPR)*, pages 1–7, 2018. 2
- [3] Noor Al-Shakarji, Ke Gao, Filiz Bunyak, Hadi Aliakbarpour, Erik Blasch, Priya Narayanan, Guna Seetharaman, and Kannappan Palaniappan. Impact of georegistration accuracy on wide area motion imagery object detection and tracking. In *International Conference on Information Fusion (FUSION)*, pages 1–8, 2021. 2
- [4] Noor M. Al-Shakarji, Filiz Bunyak, Guna Seetharaman, and Kannappan Palaniappan. Multi-object tracking cascade with multi-step data association and occlusion handling. In *2018 15th IEEE International Conference on Advanced Video and Signal Based Surveillance (AVSS)*, pages 1–6, 2018. 3
- [5] Nigar Anzar, Rahil Hasan, Manshi Tyagi, Neelam Yadav, and Jagriti Narang. Carbon nanotube-a review on synthesis, properties and plethora of applications in the field of biomedical science. *Sensors International*, 1:100003, 2020. 1
- [6] Elaheh Azizian-Farsani, Mohammad Rouhi Moghanlou, Ali Mahmoudi, Peyton J Wilson, and Michael M Khonsari. On the optimization of fatigue limit in additively manufactured

- fiber reinforced polymer composites. *Progress in Additive Manufacturing*, pages 1–20, 2025. 1
- [7] Rina Bao, Noor M. Al-Shakarji, Filiz Bunyak, and Kannappan Palaniappan. DMNet: Dual-stream marker guided deep network for dense cell segmentation and lineage tracking. In *IEEE International Conference on Computer Vision (ICCV) Workshops*, pages 3361–3370, 2021. 2
- [8] Axel Barroso-Laguna and Krystian Mikolajczyk. Key. net: Keypoint detection by handcrafted and learned cnn filters revisited. *IEEE transactions on pattern analysis and machine intelligence*, 45(1):698–711, 2022. 2
- [9] Rachel Carter, Benjamin Davis, Landon Oakes, Matthew R Maschmann, and Cary L Pint. A high areal capacity lithium–sulfur battery cathode prepared by site-selective vapor infiltration of hierarchical carbon nanotube arrays. *Nanoscale*, 9(39):15018–15026, 2017. 1
- [10] Nicolas Chenouard, Ihor Smal, Fabrice De Chaumont, Martin Maška, Ivo F Sbalzarini, Yuanhao Gong, Janick Cardinale, Craig Carthel, Stefano Coraluppi, Mark Winter, et al. Objective comparison of particle tracking methods. *Nature methods*, 11(3):281–289, 2014. 5
- [11] Megha Choudhary, Aaruni Sharma, S Aravind Raj, Mohamed Thariq Hameed Sultan, David Hui, and Ain Umaira Md Shah. Contemporary review on carbon nanotube composites and their impact on multifarious applications. *Nanotechnology Reviews*, 11(1):2632–2660, 2022. 1
- [12] Daniel DeTone, Tomasz Malisiewicz, and Andrew Rabinovich. Superpoint: Self-supervised interest point detection and description. In *IEEE Conference on Computer Vision and Pattern Recognition (CVPR)*, pages 224–236, 2018. 2
- [13] Carl Doersch, Yi Yang, Mel Vecerik, Dilara Gokay, Ankush Gupta, Yusuf Aytar, Joao Carreira, and Andrew Zisserman. Tapir: Tracking any point with per-frame initialization and temporal refinement. In *IEEE Conference on Computer Vision and Pattern Recognition (CVPR)*, pages 10061–10072, 2023. 2, 6
- [14] MA Eltaher, Alaa A Abdelrahman, and Ismail Esen. Dynamic analysis of nanoscale timoshenko cnts based on doublet mechanics under moving load. *The European Physical Journal Plus*, 136(7):705, 2021. 2
- [15] Ke Gao, Hadi AliAkbarpour, Kannappan Palaniappan, and Guna Seetharaman. Evaluation of feature matching in aerial imagery for structure-from-motion and bundle adjustment. In *SPIE Geospatial Informatics, Motion Imagery, and Network Analytics VIII*, pages 139–145, 2018. 3
- [16] Ke Gao, Shizeng Yao, Hadi AliAkbarpour, Sanjeev Agarwal, Guna Seetharaman, and Kannappan Palaniappan. Sensitivity of multiview 3D point cloud reconstruction to compression quality and image feature detectability. In *IEEE Applied Imagery Pattern Recognition Workshop (AIPR)*, pages 1–6, 2019. 3
- [17] Ke Gao, Hadi Aliakbarpour, Gunasekaran Seetharaman, and Kannappan Palaniappan. DCT-based local descriptor for robust matching and feature tracking in wide area motion imagery. *IEEE Geoscience and Remote Sensing Letters*, 18(8):1441–1445, 2020. 3
- [18] Taher Hajilounezhad, Zakariya A Oraibi, Ramakrishna Surya, Filiz Bunyak, Matthew R Maschmann, Prasad Calyam, and Kannappan Palaniappan. Exploration of carbon nanotube forest synthesis-structure relationships using physics-based simulation and machine learning. In *IEEE Applied Imagery Pattern Recognition Workshop (AIPR)*, pages 1–8, 2019. 1
- [19] Taher Hajilounezhad, Rina Bao, Kannappan Palaniappan, Filiz Bunyak, Prasad Calyam, and Matthew R Maschmann. Predicting carbon nanotube forest attributes and mechanical properties using simulated images and deep learning. *NPJ Computational Materials*, 7(1):134, 2021. 1
- [20] Adam W Harley, Zhaoyuan Fang, and Katerina Fragkiadaki. Particle video revisited: Tracking through occlusions using point trajectories. In *European Conference on Computer Vision (ECCV)*, pages 59–75. Springer, 2022. 2
- [21] Nikita Karaev, Ignacio Rocco, Benjamin Graham, Natalia Neverova, Andrea Vedaldi, and Christian Rupprecht. CoTracker: It is better to track together. In *European Conference on Computer Vision (ECCV)*, pages 18–35. Springer, 2024. 2, 5, 6
- [22] Prashanth Reddy Kotha, Minasadat Attari, Matthew Maschmann, and Filiz Bunyak. Deep style transfer for generation of photo-realistic synthetic images of cnt forests. In *2023 IEEE Applied Imagery Pattern Recognition Workshop (AIPR)*, pages 1–7. IEEE, 2023. 1
- [23] Yashas Kuchimanchi, Gani Rahmon, Tania Banerjee, Sar-taj Sahni, Guna Seetharaman, and Kannappan Palaniappan. Optimizing short-term data association for multiple object tracking. In *SPIE Geospatial Informatics XV*, pages 10–32, 2025. 3
- [24] Philipp Lindenberger, Paul-Edouard Sarlin, and Marc Pollefeys. Lightglue: Local feature matching at light speed. In *IEEE Conference on Computer Vision and Pattern Recognition (CVPR)*, pages 17627–17638, 2023. 2
- [25] Jian Liu, Wenjie Kuang, Jiaqiang Liu, Zhenguo Gao, Sohrab Rohani, and Junbo Gong. In-situ multi-phase flow imaging for particle dynamic tracking and characterization: Advances and applications. *Chemical Engineering Journal*, 438:135554, 2022. 2
- [26] David G Lowe. Distinctive image features from scale-invariant keypoints. *International Journal of Computer Vision (IJCV)*, 60:91–110, 2004. 2
- [27] Jiayi Ma, Xingyu Jiang, Aoxiang Fan, Junjun Jiang, and Junchi Yan. Image matching from handcrafted to deep features: A survey. *International Journal of Computer Vision*, 129(1):23–79, 2021. 2
- [28] Mohammad Rouhi Moghanlou, Elaheh Azizian-Farsani, Ali Mahmoudi, and Michael M Khonsari. Accelerated fatigue characterization of additively manufactured continuous carbon fiber reinforced thermoplastic: A thermodynamic approach. *Composites Part A: Applied Science and Manufacturing*, 192:108805, 2025. 1
- [29] Lida Najmi and Zhong Hu. Thermal properties of carbon nanotubes reinforced epoxy matrix composites by molecular dynamic simulations. In *APS Division of Atomic, Molecular and Optical Physics Meeting Abstracts*, pages C11–007, 2024. 1
- [30] Lida Najmi and Zhong Hu. Effects of key parameters on thermal conductivity of carbon nanotube–epoxy composites

- by molecular dynamics simulations. *Journal of Composites Science*, 9(4):159, 2025. 1
- [31] Jay M Newby, Alison M Schaefer, Phoebe T Lee, M Gregory Forest, and Samuel K Lai. Convolutional neural networks automate detection for tracking of submicron-scale particles in 2d and 3d. *Proceedings of the National Academy of Sciences*, 115(36):9026–9031, 2018. 2
- [32] Nguyen P Nguyen, Ramakrishna Surya, Matthew Maschmann, Prasad Calyam, Kannappan Palaniappan, and Filiz Bunyak. Self-supervised orientation-guided deep network for segmentation of carbon nanotubes in sem imagery. In *Springer European Conference on Computer Vision (ECCV)*, pages 412–428, 2022. 1
- [33] Nguyen P Nguyen, Ramakrishna Surya, Prasad Calyam, Kannappan Palaniappan, Matthew Maschmann, and Filiz Bunyak. Cnt-nerf: Carbon nanotube forest depth layer decomposition in sem imagery using generative adversarial networks. In *IEEE Conference on Computer Vision and Pattern Recognition (CVPR)*, pages 3428–3437, 2023. 1
- [34] Vladimir Pimonov, Huy-Nam Tran, Léonard Monniello, Saïd Tahir, Thierry Michel, Renaud Podor, Michaël Odorico, Christophe Bichara, and Vincent Jourdain. Dynamic instability of individual carbon nanotube growth revealed by in situ homodyne polarization microscopy. *Nano Letters*, 21(19):8495–8502, 2021. 2
- [35] Bakhtiyor Rasulev. Ecotoxicological qsar modeling of nanomaterials: Methods in 3d-qsars and combined docking studies for carbon nanostructures. *Ecotoxicological QSARs*, pages 215–233, 2020. 1
- [36] Kaveh Safavigerdini, Koundinya Nouduri, Ramakrishna Surya, Andrew Reinhard, Zach Quinlan, Filiz Bunyak, Matthew R Maschmann, and Kannappan Palaniappan. Predicting mechanical properties of carbon nanotube (cnt) images using multi-layer synthetic finite element model simulations. In *IEEE International Conference on Image Processing (ICIP)*, pages 3264–3268, 2023. 1
- [37] Kaveh Safavigerdini, Ramakrishna Surya, Andrew Reinhard, Zach Quinlan, Filiz Bunyak, Matthew R Maschmann, and Kannappan Palaniappan. Creating semi-quanta multi-layer synthetic cnt images using cyclegan. In *IEEE Applied Imagery Pattern Recognition Workshop (AIPR)*, pages 1–6, 2023. 1
- [38] Paul-Edouard Sarlin, Daniel DeTone, Tomasz Malisiewicz, and Andrew Rabinovich. Superglue: Learning feature matching with graph neural networks. In *IEEE Conference on Computer Vision and Pattern Recognition (CVPR)*, pages 4938–4947, 2020. 2
- [39] Johannes L Schonberger, Hans Hardmeier, Torsten Sattler, and Marc Pollefeys. Comparative evaluation of hand-crafted and learned local features. In *Proceedings of the IEEE conference on computer vision and pattern recognition*, pages 1482–1491, 2017. 2
- [40] Hao Shen, Lawrence J Tazuin, Rashad Baiyasi, Wenxiao Wang, Nicholas Moringo, Bo Shuang, and Christy F Landes. Single particle tracking: from theory to biophysical applications. *Chemical reviews*, 117(11):7331–7376, 2017. 2
- [41] Sijia Shen, Lingwei Yang, Chuanyun Wang, and Liming Wei. Effect of cnt orientation on the mechanical property and fracture mechanism of vertically aligned carbon nanotube/carbon composites. *Ceramics International*, 46(4):4933–4938, 2020. 1
- [42] Ramakrishna Surya and Matthew R Maschmann. Using electrical resistance as a diagnostic during process-structure-property investigation of cnt forests. In *ASME International Mechanical Engineering Congress and Exposition*, page V003T03A020, 2023. 1
- [43] Ramakrishna Surya, Gordon L Koerner, Taher Hajilounezhad, Kaveh Safavigerdini, Prasad Calyam, Filiz Bunyak, Kannappan Palaniappan, and Matthew R Maschmann. Measurements of cnt forest self-assembly from in-situ esem synthesis. *arXiv preprint arXiv:2402.19336*, 2024. 1
- [44] Ramakrishna Surya, Gordon L Koerner, Taher Hajilounezhad, Kaveh Safavigerdini, Martin Spies, Prasad Calyam, Filiz Bunyak, Kannappan Palaniappan, and Matthew R Maschmann. Cnt forest self-assembly insights from in-situ esem synthesis. *Carbon*, 229:119439, 2024. 1
- [45] Imad Eddine Toubal, Noor Al-Shakarji, D. D. W. Cornelison, and Kannappan Palaniappan. Ensemble deep learning object detection fusion for cell tracking, mitosis, and lineage. *IEEE Open Journal of Engineering in Medicine and Biology*, 5:443–458, 2024. 2
- [46] Michał Tyszkiewicz, Pascal Fua, and Eduard Trulls. Disk: Learning local features with policy gradient. *Advances in Neural Information Processing Systems (NeurIPS)*, 33:14254–14265, 2020. 2
- [47] Bahram Yaghooti, Ali Siahi Shadbad, Kaveh Safavi, and Hassan Salarieh. Adaptive synchronization of uncertain fractional-order chaotic systems using sliding mode control techniques. *Proceedings of the Institution of Mechanical Engineers, Part I: Journal of Systems and Control Engineering*, 234(1):3–9, 2020. 2
- [48] Bahram Yaghooti, Kaveh Safavigerdini, Reza Hajiloo, and Hassan Salarieh. Stabilizing unstable periodic orbit of unknown fractional-order systems via adaptive delayed feedback control. *Proceedings of the Institution of Mechanical Engineers, Part I: Journal of Systems and Control Engineering*, 238(4):693–703, 2024. 2
- [49] Xiaoming Zhao, Xingming Wu, Weihai Chen, Peter CY Chen, Qingsong Xu, and Zhengguo Li. Aliked: A lighter keypoint and descriptor extraction network via deformable transformation. *IEEE Transactions on Instrumentation and Measurement*, 2023. 2
- [50] Weiwei Zhou, Lei Ding, Sungwoo Yang, and Jie Liu. Orthogonal orientation control of carbon nanotube growth. *Journal of the American Chemical Society*, 132(1):336–341, 2010. 1
- [51] Tuyuan Zhu, Ying Sha, Huiwen Zhang, Yingchong Huang, Xuehui Gao, Min Ling, and Zhan Lin. Embedding fe₃c and fe₃n on a nitrogen-doped carbon nanotube as a catalytic and anchoring center for a high-area-capacity li-s battery. *ACS Applied Materials & Interfaces*, 13(17):20153–20161, 2021. 1